Bulletin of the Seismological Society of America, Vol. 107, No. 3, pp. 1240–1253, June 2017, doi: 10.1785/0120160255

Ⓔ

Alternative Rupture-Scaling Relationships for Subduction Interface and Other Offshore Environments

by Trevor I. Allen* and Gavin P. Hayes

Abstract Alternative fault-rupture-scaling relationships are developed for M_w 7.1–9.5 subduction interface earthquakes using a new database of consistently derived finite-fault rupture models from teleseismic inversion. Scaling relationships are derived for rupture area, rupture length, rupture width, maximum slip, and average slip. These relationships apply width saturation for large-magnitude interface earthquakes (approximately $M_w > 8.6$) for which the physical characteristics of subduction zones limit the depth extent of seismogenic rupture, and consequently, the down-dip limit of strong ground motion generation. On average, the down-dip rupture width for interface earthquakes saturates near 200 km (196 km on average). Accordingly, the reinterpretation of rupture-area scaling for subduction interface earthquakes through the use of a bilinear scaling model suggests that rupture asperity area is less well correlated with magnitude for earthquakes $M_w > 8.6$. Consequently, the size of great-magnitude earthquakes appears to be more strongly controlled by the average slip across asperities.

The sensitivity of the interface scaling relationships is evaluated against geographic region (or subduction zone) and average dip along the rupture interface to assess the need for correction factors. Although regional perturbations in fault-rupture scaling could be identified, statistical significance analyses suggest there is little rationale for implementing regional correction factors based on the limited number of interface rupture models available for each region.

Fault-rupture-scaling relationships are also developed for intraslab (within the subducting slab), extensional outer-rise and offshore strike-slip environments. For these environments, the rupture width and area scaling properties yield smaller dimensions than interface ruptures for the corresponding magnitude. However, average and maximum slip metrics yield larger values than interface events. These observations reflect both the narrower fault widths and higher stress drops in these faulting environments. Although expressing significantly different rupture-scaling properties from earthquakes in subduction environments, the characteristics of offshore strike-slip earthquake ruptures compare similarly to commonly used rupture-scaling relationships for onshore strike-slip earthquakes.

Electronic Supplement: Table of rupture parameters.

Introduction

Fault-rupture-scaling relationships have numerous applications in both earthquake- and tsunami-hazard analyses. For example, modern event-based probabilistic seismic-hazard analysis (PSHA) codes rely on these relationships to simulate ground-motion fields (GMFs) from randomized pseudoruptures within areal source zones or to scale floating ruptures across a predefined fault surface (e.g., Pagani *et al.*, 2014). If not assuming characteristic earthquake ruptures, the rupture geometries are calculated using fault-scaling relationships (e.g., Wells and Coppersmith, 1994, and others). The GMFs are then determined by these ruptures in concert with ground-motion models that are calibrated to the closest distance to the rupture plane. Rupture-scaling relationships also play a key role in developing GMFs for earthquake impact scenarios and probabilistic seismic risk assessments, for paleoseismological studies, and for informing catalog declustering algorithms.

*Now at Geoscience Australia, GPO Box 378, Canberra, Australian Capital Territory 2601, Australia.

Table 1
Published Fault-Rupture-Scaling Relationships for Subduction Environments

Reference	S	S_a	L	W	D_{max}	D_{av}	Intraslab
Wells and Coppersmith (1994)	✓		✓	✓	✓*	✓*	
Murotani *et al.* (2008)†	✓	✓				✓	
Blaser *et al.* (2010)			✓	✓			
Leonard (2010)†	✓		✓		✓		
Strasser *et al.* (2010)	✓		✓	✓			✓
Murotani *et al.* (2013)†	✓	✓				✓	
Skarlatoudis *et al.* (2016)†	✓	✓		✓	✓	✓	
Present study	✓		✓	✓	✓	✓	✓

*Poorly constrained for reverse-faulting events.
†Self-similar scaling relationships.

In deterministic tsunami assessments, fault-rupture-scaling relationships are an important component for determining the extent of coastline that may be impacted by tsunami through the use of both average slip and length scaling of fault rupture along a subduction interface. Probabilistic tsunami-hazard assessments (PTHAs) extend this application by simulating pseudoruptures for a synthetic catalog of possible subduction interface tsunami sources (e.g., Sørensen *et al.*, 2012; Horspool *et al.*, 2014; Thio and Li, 2015).

Several fault-rupture-scaling relationships have now been developed specifically for subduction environments (Murotani *et al.*, 2008, 2013; Blaser *et al.*, 2010; Strasser *et al.*, 2010; Somerville *et al.*, 2015; Skarlatoudis *et al.*, 2016). These authors provide a range of equations to resolve various properties for subduction interface and in-slab ruptures, including rupture area (S), rupture asperity area (S_a), rupture length (L), rupture width (W), maximum slip (D_{max}), and average slip (D_{av}). Some of the aforementioned scaling relations are purely empirical, whereas others invoke self-similar fault-scaling principles—see Blaser *et al.* (2010) and Strasser *et al.* (2010) for further discussion on the comparison of self-similar and non-self-similar scaling. Table 1 indicates scaling relations appropriate for subduction environments and the specific rupture properties that can be resolved.

One disadvantage of the previous studies is that they use fault-rupture data from multiple sources, which are often derived using disparate methods and assumptions. Therefore, uncertainties arising from differences in modeling techniques and parameterization can affect the confidence in derivative products such as rupture-scaling relationships. These uncertainties can be reduced, to a certain extent, by comparing only those models that have been generated using a consistent modeling approach. The present study uses a large database of finite-fault-rupture models (FFRMs) from recent earthquakes that have been developed using a uniform teleseismic inversion method (Hayes *et al.*, 2015).

In both PSHA and PTHA, it is often appropriate to use multiple methods and models to account for the epistemic uncertainty. Herein, we develop alternative fault-rupture-scaling relationships that are appropriate for subduction and other offshore environments that could be used independently, or in concert with alternative scaling relationships in a probabilistic framework.

Finite-Fault Rupture Models

Many authors contributed FFRMs for significant global earthquakes (Mai and Thingbaijam, 2014, and references therein). While an excellent resource, many of these contributed models have been developed using disparate approaches and assumptions. Therefore, uncertainties arising from differences in modeling techniques and parameterization can affect the confidence in derivative products when using multiple, different models.

Hayes *et al.* (2015) has developed an FFRM database for most of the $M_w \geq 7.5$ global earthquakes since 1990. All rupture models in the database use uniform teleseismic inversion-modeling techniques and parameterization. Deep earthquakes (> 300 km) are excluded from the dataset, because of their different rupture kinematics compared with shallow (< 70 km) and intermediate-depth (70–300 km) earthquakes. We use these FFRMs to develop alternative scaling relationships for interface and intraslab subduction zone earthquakes. Additionally, scaling relationships based on limited offshore strike-slip and subduction outer-rise events are also provided. In total, 99 FFRMs from the Hayes *et al.* (2015) database are used in these analyses (Ⓔ Table S1, available in the electronic supplement to this article).

Because the parameter space used to invert for FFRMs often exceeds the area of primary slip and thus that of strong-motion generation, it is necessary to first trim the FFRMs to an effective rupture area. A consistent two-step process is developed that trims low-slip subfault areas that are not likely to generate strong ground shaking hazard. First, we attempt to remove noise from each FFRM. The simplification of complex earthquake-rupture processes to a simple planar surface (or multiple planar surfaces), rupturing during an expanding but finite slip pulse together with complexities in seismic wavepaths, can introduce artifacts into FFRMs. These effects are more commonly observed at the later time-steps in the modeling process. To mitigate noise artifacts from the rupture models, a maximum duration of rupture was manually assigned to all earthquakes within the Hayes dataset, based on analyses of the more stable earthquake source time functions associated with each FFRM. All slips on FFRM subfaults at time-steps greater than the assigned rupture duration were set to zero. The assigned rupture durations for the earthquakes studied are indicated in Ⓔ Table S1.

Next, with FFRM noise removed, we trim subfaults that have slip (D_{ij}) less than a given slip threshold D_{lim}, in which

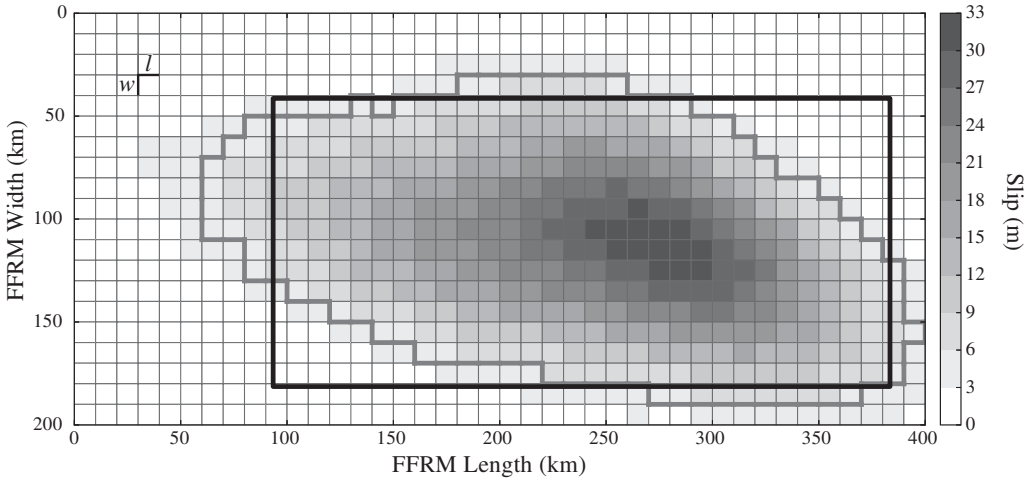

Figure 1. Schematic of fault trimming process. A synthetic finite-fault rupture model (FFRM) is plotted showing the slip for each subfault of length l and width w. The thick gray line bounds the maximum and minimum subfault indexes for each column i and row j for which the slip $D_{ij} \geq D_{\text{lim}}$. The thick black line represents the effective rupture dimensions used for L and W.

$$D_{\text{lim}} = \xi \times D_{\text{max}}. \quad (1)$$

In a recent publication, Ye *et al.* (2016) recommended a trimming threshold of $\xi = 0.15$ based on comparisons between static and energy-related stress drops. Although the choice of ξ is still somewhat arbitrary, the chosen value is expected to preserve the areas of significant slip on a fault plane that are likely to generate strong ground shaking.

The process for trimming the FFRMs is outlined below and illustrated in Figure 1. To estimate the overall down-dip rupture width W, we first iteratively step though each subfault column i along the strike direction and find the effective column width W_i. For each row j in each column i, the upper and lower subfaults with a slip D_{ij} greater than, or equal to, the minimum slip D_{lim} are identified.

For each down-dip subfault ($j = 1, 2, \ldots, n$) with width w, the effective down-dip widths for each column i are

$$W_i = \max[z_{b,i1}, z_{b,i2}, \ldots, z_{b,in}] - \min[z_{u,i1}, z_{u,i2}, \ldots, z_{u,in}], \quad (2)$$

in which $z_{b,ij}$ is the lower width limit (or bottom of down-dip rupture),

$$z_{b,ij} = \begin{cases} j \times w | D_{ij} \geq D_{\text{lim}} \\ 0 | D_{ij} < D_{\text{lim}} \end{cases} \quad \text{for } j = 1, 2, \ldots, n, \quad (3)$$

and $z_{u,ij}$ is the upper width limit (or top of down-dip rupture),

$$z_{u,ij} = \begin{cases} (j-1) \times w | D_{ij} \geq D_{\text{lim}} \\ \infty | D_{ij} < D_{\text{lim}} \end{cases} \quad \text{for } j = 1, 2, \ldots, n. \quad (4)$$

The effective rupture width is then taken as the 75th percentile of the distribution $[W_1, W_2, \ldots, W_n]$. Similarly, to determine the rupture length L, we iteratively step through each subfault row j along the dip direction. For each along-strike subfault ($i = 1, 2, \ldots, n$) with length l, the effective lengths for each row j are

$$L_j = \max[x_{2,1j}, x_{2,2j}, \ldots, x_{2,nj}] - \min[x_{1,1j}, x_{1,2j}, \ldots, x_{1,nj}], \quad (5)$$

in which $x_{2,ij}$ is the upper row limit,

$$x_{2,ij} = \begin{cases} i \times l | D_{ij} \geq D_{\text{lim}} \\ 0 | D_{ij} < D_{\text{lim}} \end{cases} \quad \text{for } i = 1, 2, \ldots, n, \quad (6)$$

and $x_{1,ij}$ is the lower row limit,

$$x_{1,ij} = \begin{cases} (j-1) \times w | D_{ij} \geq D_{\text{lim}} \\ \infty | D_{ij} < D_{\text{lim}} \end{cases} \quad \text{for } i = 1, 2, \ldots, n. \quad (7)$$

The effective rupture length L is then taken as the 75th percentile of the distribution $[L_1, L_2, \ldots, L_n]$. The rupture area S for single-segment models is the product of L and W. The maximum slip D_{max} is not dependent on the trimming process. Given that subfault areas are not equal between models, D_{max} is a function of the rupture model resolution. However, the average slip D_{av} is modified such that the total non-trimmed slip is averaged across the nontrimmed subfaults. Figure 1 shows a schematic diagram of the FFRM trimming process for a single-segment rupture.

Although the majority of the dataset used in this study are single-segment FFRMs, where it is appropriate, multisegment FFRMs have been evaluated (Hayes *et al.* 2015). For multi-segment models, each segment is individually trimmed using the aforementioned process. The effective rupture width W is then taken as the total down-dip extent of the combined, trimmed segments. The effective rupture length L is taken as the lateral extent of the trimmed rupture segments. The total rupture area S is the summed area of each fault segment k:

$$S = \sum_{k=1}^{N} L_k \times W_k. \tag{8}$$

Because the FFRM dataset of Hayes *et al.* (2015) is limited to events occurring since 1990, it lacks many of the largest-magnitude subduction events that occurred in instrumental times. To supplement the current dataset, we include fault-rupture models from other studies, including the 1952 M_w 8.9 Kamchatka (Johnson and Satake, 1999), the 1957 M_w 8.6 Aleutian Islands (Johnson *et al.*, 1994), the 1960 M_w 9.5 Concepción (Moreno *et al.*, 2009), and the 1964 M_w 9.3 Prince William Sound (Johnson *et al.*, 1996) earthquakes. Rupture dimensions for these earthquakes were taken from published rupture models (as indicated above). The effective dimensions of strong-motion generation for these historical events were taken as 85% of the model extent. This value is approximately commensurate with the average trimming percentage from the analysis of large earthquakes (approximately $M_w \geq 8.0$) in the Hayes *et al.* (2015) FFRM dataset (see Ⓔ Table S1). Hayes *et al.* (2015) did not attempt to model the great 2004 M_w 9.2 Sumatra earthquake using teleseismic inversion techniques because of the extremely long duration of this event. Consequently, we include the model of Rhie *et al.* (2007), which uses joint inversion of teleseismic and Ground Positioning System static offset observations. The FFRM of Rhie *et al.* (2007) was processed in a similar manner to those of Hayes *et al.* (2015) to obtain the effective rupture parameters. Although every effort was made to use rupture parameters determined from a consistently derived teleseismic inversion approach, the historical earthquakes and the 2004 Sumatra event were considered to be critical for characterizing the rupture-scaling parameters for great ($M_w > 8.5$) earthquakes.

The parameters of rupture area (S), rupture length (L), rupture width (W), maximum slip (D_{max}), and average slip (D_{av}) were extracted from the trimmed FFRMs for regression analysis. These parameters were categorized by event type (e.g., interface, intraslab, outer rise, and offshore strike slip) to develop rupture-scaling relationships with earthquake magnitude M_w. Seismic moment $M_0 (\propto M_w)$ is related to both the rupture area and average slip according to the standard formulation

$$M_0 = \mu S D_{av} \tag{9}$$

(Aki, 1966), in which μ is the shear modulus (rigidity).

The geographic region and average slab dip (where available for interface events) was also determined to explore subduction-zone-specific correction factors. Rupture parameters for the earthquakes used to develop scaling models herein are presented in Ⓔ Table S1. The earthquakes are mapped in Figure 2, in which the corresponding event indexes are consistent with Ⓔ Table S1.

Fault-Scaling Relationships for Interface Ruptures

Weighted orthogonal regression methods were used to develop scaling relationships for interface subduction earthquakes

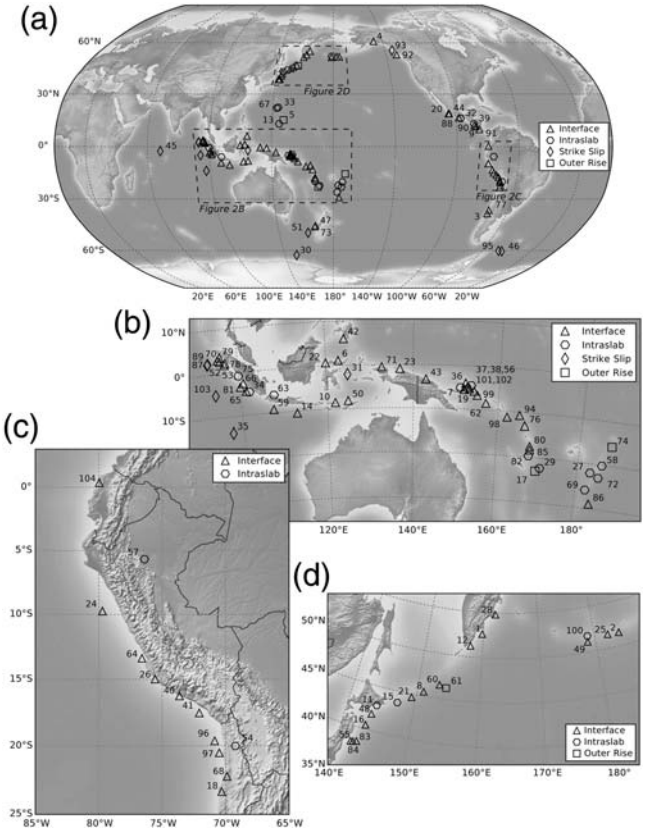

Figure 2. (a) Global distribution of epicenters and rupture types for earthquakes used in this study. Subplots show the detailed distribution of earthquakes in (b) the southeast Asia and the southwest Pacific region; (c) South America; and (d) the Kuril-Aleutian island arc region. The numbering of epicenters is consistent with the event index in Ⓔ Table S1, available in the electronic supplement to this article.

using the trimmed FFRMs for events between M_w 7.1 and 9.5. The orthogonal regression technique accounts for measurement errors in the x and y variables, and the method provides a unique solution that is fully reversible. Larger-magnitude earthquakes were given a higher weight in the regressions, owing to their lower frequency of occurrence. Standard deviations, σ_{ODR}, were assigned to the x and y variables, and these values are converted to regression weights by taking the inverse of their squares (see Data and Resources). For both x and y variables, σ_{ODR} is taken as 0.2 for $M_w < 7.5$ and as 0.1 for $M_w > 8.0$, respectively. Values for σ_{ODR} are linearly interpolated between 0.2 and 0.1 for intermediate magnitudes.

A linear relationship is developed between rupture length and moment magnitude (Fig. 3a). The relationship is generally consistent with other published length-scaling relationships for larger magnitudes but tends to yield shorter rupture lengths at small magnitudes. The coefficients for the L–M_w relationship are provided in Table 2.

Tajima *et al.* (2013) and Somerville *et al.* (2015) suggested that the down-dip rupture width of subduction interface earthquakes may be limited to about 200 km. Although this hypothesis is based on sparse empirical observations from large (approximately $M_w > 8.4$) megathrust earthquakes,

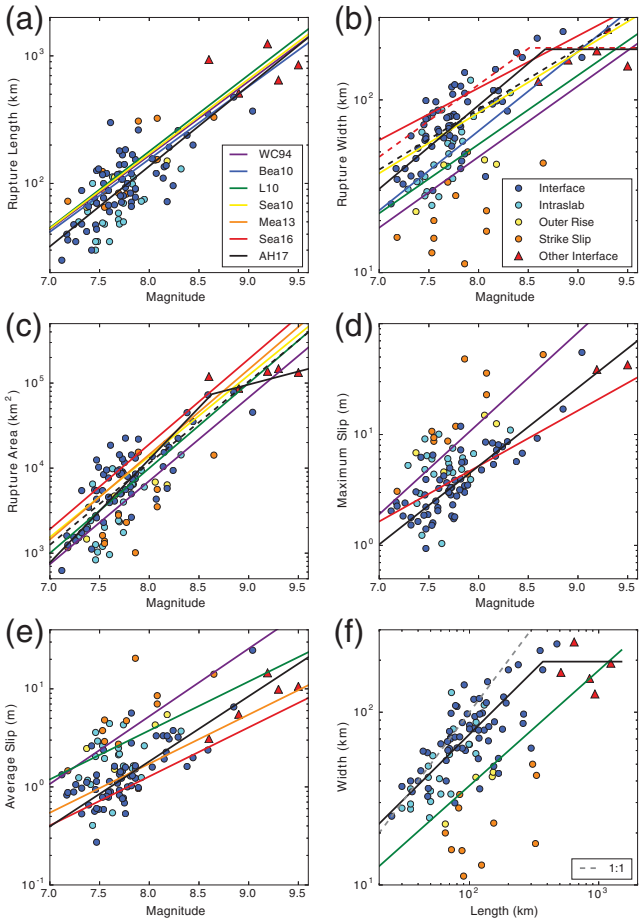

Figure 3. Orthogonal regressions for subduction interface rupture parameters from the present study (AH17). Relationships are shown between earthquake magnitude M_w and (a) rupture length L, (b) rupture width W, (c) rupture area S, (d) maximum slip D_{max}, and (e) average slip D_{av}, where appropriate, both linear (dashed) and bilinear (solid) fault-scaling relations are provided for width and area scaling. (f) The W–L relationship for interface earthquakes is also shown together with 1:1 L–W scaling (dashed line). The regressions were performed using *interface* and *other interface* data classes, and the coefficients for these relationships are given in Table 2. Although not used in the regressions, data points for intraslab, outer-rise, and offshore strike-slip events are also shown. Where applicable, the AH17 scaling relationships are compared with other published models, including Wells and Coppersmith (1994; WC94) (a–c) reverse-slip and (d,e) all rupture types; Blaser *et al.* (2010; Bea10) reverse-slip; Leonard (2010; L10) dip-slip; Strasser *et al.* (2010; Sea10) interface; Murotani *et al.* (2013; Mea13); and Skarlatoudis *et al.* (2016; Sea16) (b) non-self-similar for W and self-similar otherwise.

the notion has sound observational and theoretical basis. Hyndman *et al.* (1997) suggested that the down-dip seismic limit for most subduction zones appears to agree with either a maximum temperature of 350°C or the interface intersection with the fore-arc serpentinized mantle. However, the saturation of down-dip rupture widths for large megathrust interface subduction earthquakes most likely varies from one subduction zone to another (Somerville *et al.*, 2015). Indeed, Hayes *et al.* (2012) quantified seismogenic zone width and observed significant variation between subduction zones, whereas Heuret *et al.* (2011) suggest the maximum depth of seismogenic rupture is dependent on the velocity and thermal properties of the subducting slab.

Many interface subduction fault-rupture-scaling relations fail to consider width saturation in their parameterization. However, models recently proposed by Allen and Hayes (2015) and Somerville *et al.* (2015) provide alternative scaling relationships that apply rupture width saturation. Somerville *et al.* (2015), updated in Skarlatoudis *et al.* (2016), develop a non-self-similar relation that scales with seismic moment M_0 and applies a down-dip rupture width saturation of 200 km with a hinge magnitude near M_w 8.4, based on the observations of Tajima *et al.* (2013) and their own data. Preliminary analysis of the empirical data gathered by Allen and Hayes (2015) and updated in this study also suggested saturation of down-dip rupture width (W_2) with increasing magnitude for interface earthquakes. We apply a bilinear orthogonal regression of the W_2–M_w data using a fixed gradient of zero above the hinge magnitude M_h. The hinge magnitude was empirically determined to be M_w 8.67 with an average saturation width of 196 km (Fig. 3b). However, rupture widths of as much as ~250 km are possible for shallowly dipping subduction interfaces (e.g., the Alaska subduction zone). There is significant variability among the W-scaling models of other published studies. Although the dataset used in the present study is largely independent of those used in other studies, the preferred bilinear W_2-scaling model developed herein appears to be most consistent with the linear model of Strasser *et al.* (2010) at low magnitudes and the bilinear non-self-similar scaling model of Skarlatoudis *et al.* (2016) at large magnitudes (with a similar average upper limit). Although the W_2-scaling model is recommended, a linear (W_1) relationship between W and M_w is provided for comparison with other published models. The linear W_1-scaling model was most comparable to the linear model of Strasser *et al.* (2010).

Although down-dip rupture width will saturate with magnitude, the rupture area (S) will continue to grow as the rupture length increases, albeit at a slower rate. Consequently, we also apply an orthogonal bilinear regression to resolve rupture area S_2 to M_w relationships. Because the trimmed rupture areas of great megathrust earthquakes can be determined from multisegment fault inversions, often with differing rupture widths along the fault strike, we do not enforce the same M_h as was determined from the bilinear W_2–M_w relationship. However, the hinge magnitude at which the gradient of the preferred bilinear S_2–M_w relationship changes is similar to the independently determined W_2–M_w relationship: M_w 8.63 (Fig. 3c). The use of the bilinear S_2 model suggests that rupture area increases more rapidly than predicted by existing rupture-area-scaling models at magnitudes less than M_h but more slowly above M_h. A linear S_1-scaling model was also developed for completeness. The linear S_1-scaling model is most similar to the linear model of Leonard (2010).

The advantage of using a consistently derived suite of FFRMs is that the magnitude scaling of rupture slip can be easily determined from the discretized subfaults. Two slip-

Table 2
Interface-Rupture-Scaling Coefficients Determined from Orthogonal Regression

Function	A	b	σ_x*	σ_y*	Condition†
$\log L = a + b \times M_w$ (km)	−2.90	0.63	0.182	0.289	–
$\log W_1 = a + b \times M_w$ (km)	−0.86	0.35	0.142	0.405	–
$\log W_2 = a + b \times M_w$ (km)	−1.91	0.48	0.137	0.294	$M_w \leq 8.67$ and $W_2 \leq 196$
	2.29	0.00			$M_w > 8.67$
$\log S_1 = a + b \times M_w$(km^2)	−3.63	0.96	0.255	0.266	–
$\log S_2 = a + b \times M_w$(km^2)	−5.62	1.22	0.256	0.267	$M_w \leq 8.63$ and $S_2 \leq 74,000$
	2.23	0.31			$M_w > 8.63$ and $74,000 < S_2 \leq 137,000$
$\log D_{max} = a + b \times M_w$ (m)	−4.94	0.71	0.179	0.254	–
$\log D_{av} = a + b \times M_w$ (m)	−5.05	0.66	0.209	0.315	–
$\log W = a + b \times \log L$ (km)	0.39	0.74	0.156	0.098	$W \leq 196$ or $L \leq 369$
	2.29	0.00			$L > 369$

All logarithms are to base 10.

*σ_x and σ_y refer to the standard deviation of the variables on the left and right side of the equation from the orthogonal regression, respectively. Standard deviations for rupture geometries are in $\log_{10}$ units, whereas magnitudes are linear.

†All interface relationships are valid from $7.1 \leq M_w \leq 9.5$.

magnitude models are developed: maximum slip, D_{max} (Fig. 3d), and average slip over the trimmed fault area, D_{av} (Fig. 3e). In addition to L and W scaling, relationships for fault slip are particularly useful for tsunami-hazard modeling and rupture deformation studies. The maximum slip for each earthquake was taken from the FFRM subfault with the largest displacement. It should be noted, however, that precise peak displacements are difficult to constrain using teleseismic data alone, given the aforementioned trade-off between slip and subfault size and between slip distribution and rupture velocity. Consequently, the implied relationships should be considered as representative of the physical process and not an absolute measure of peak slip. Although the D_{av} model has a different gradient from other published self-similar scaling models for interface earthquakes (Fig 3e), the model lies intermediate between Leonard (2010) and Skarlatoudis *et al.* (2016) and appears to better represent the average slip for great-magnitude earthquakes (approximately $M_w \geq 9.0$). The coefficients for all interface-scaling relationships are provided in Table 2.

For completeness, L–W scaling parameters are provided for interface earthquake ruptures. To provide consistency with the bilinear W_2–M_w relationship, the maximum rupture width is limited to 196 km (Fig. 3f). Rupture width scales approximately as three quarters (0.74) of the rupture length for subduction interface earthquakes for ruptures less than the average saturation width (Table 2), with rupture length and width equal near 20–30 km.

Regional Dependence of Interface Scaling

Different authors identified variations in the physical characteristics of global subduction zones, in parameters such as subduction velocity, slab age, depth of seismogenic rupture, and maximum magnitude (e.g., Heuret *et al.*, 2011; Hayes *et al.*, 2012; Schellart and Rawlinson, 2013). Using the present dataset, we investigate whether there is any regional dependence on interface-rupture-scaling properties. The dataset is assigned a region based on the definition of global subduction zones by Hayes *et al.* (2012). Figure 4 shows the variability ($\log_{10}$ residuals) in subduction interface ruptures, grouped by subduction zone, with respect to the global relations in Figure 3. For length (L), width (W_2), and area (S_2) rupture scaling, we conduct a Welch's t-test to determine whether regional differences in the residuals can be considered statistically significant. Although there may be some evidence to support regional differences in rupture-length scaling, the null hypothesis that no regional scaling differences exist cannot be rejected at the 0.05 probability level for any region or rupture metric (Table 3). Based on these analyses (and this dataset), it is difficult to justify the application of regional corrections to the scaling coefficients.

Sensitivity of Interface-Scaling Relationships to Slab Dip

The sensitivity of the scaling relationships is also evaluated against the average dip across the trimmed rupture interface. Trimmed FFRM segments were gridded into a 10×10 matrix. The interface dip was estimated at each vertex from the Slab 1.0 models of Hayes *et al.* (2012) where possible. The average dip for each trimmed FFRM was subsequently calculated. In Figure 5, interface rupture areas are plotted against magnitude and color-coded by the average slab dip. Although no significant bias in rupture scaling could be identified with the dip of the interface, a weak correlation between average dip and the magnitude of interface events was observed. Although only a very small sample over a limited time period, the data suggest that great events (approximately $M_w \geq 8.0$) that nucleate on steeply dipping subduction interfaces (approximately $\geq 25°$) may occur at lower probabilities than on shallow-dipping interfaces (approximately $\leq 25°$).

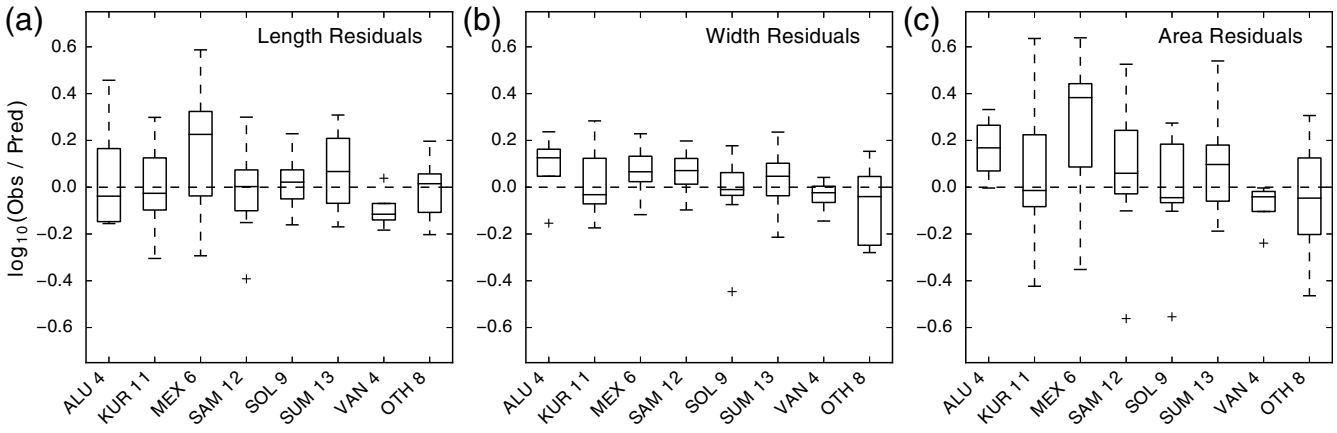

Figure 4. Box and whisker plots indicating the residuals of the scaling relationship for different subduction zones for (a) rupture length (using bilinear L_2–M_w scaling), (b) rupture width, and (c) rupture area, with respect to the global subduction interface relations in Figure 3. Three-letter codes are consistent with the definition of Hayes *et al.* (2012): ALU, Aleutian; KUR, Kuril; MEX, Mexico; SAM, South America; SOL, Solomon Islands; SUM, Sumatra; VAN, Vanuatu, and OTH, other regions with undefined slab models. The number of events per region is indicated.

Fault-Scaling Relationships for Other Rupture Types

The FFRM dataset gathered through this study includes earthquakes for other rupture settings such as intraslab, extensional outer-rise, and offshore strike-slip earthquakes. To establish whether rupture properties for these earthquake types are statistically different from those of interface earthquakes, we first examine their residuals relative to the coefficients for the interface-scaling relations from Table 2. Figure 6 shows the rupture length, width, and area residuals for each rupture type relative to the bilinear interface coefficients. With the exception of rupture length, differences between the rupture scaling of interface and noninterface earthquake types are clearly observed. A subsequent *t*-test concludes that the datasets for the noninterface event types accept the null hypothesis—that they can be treated as independent datasets—and justifies the development of alternative equations (Table 4). Owing to the sparse data coverage over a limited magnitude range for the other event types, the gradients determined through the orthogonal regression analysis on the interface data are used. The following sections discuss the development of scaling relations for each of the other rupture types.

Table 3
Regional-Rupture-Scaling Residual Statistics

	Region	$\tilde{x}$	σ	*p*-value
Rupture-length residuals	ALU	−0.04	0.25	0.821
	KUR	−0.03	0.17	0.546
	MEX	0.23	0.29	0.296
	SAM	0.00	0.17	0.524
	SOL	0.02	0.11	0.921
	SUM	0.07	0.15	0.234
	VAN	−0.12	0.08	0.069
	OTH	0.01	0.13	0.477
	ALL	0.01	0.18	–
Rupture-width residuals	ALU	0.13	0.15	0.471
	KUR	−0.03	0.14	0.802
	MEX	0.07	0.11	0.330
	SAM	0.07	0.09	0.096
	SOL	−0.01	0.16	0.411
	SUM	0.05	0.12	0.683
	VAN	−0.02	0.07	0.237
	OTH	−0.04	0.16	0.123
	ALL	0.02	0.14	–
Rupture-area residuals	ALU	0.17	0.13	0.235
	KUR	−0.01	0.29	0.840
	MEX	0.38	0.33	0.221
	SAM	0.06	0.25	0.968
	SOL	−0.04	0.24	0.472
	SUM	0.10	0.20	0.360
	VAN	−0.04	0.09	0.058
	OTH	−0.05	0.23	0.215
	ALL	0.00	0.26	–

The $\log_{10}$ regional-rupture-scaling residuals indicating the median $\tilde{x}$, standard deviation σ, and *p*-value based on the null hypothesis that the regional scaling of interface ruptures are significant.

Intraslab Rupture Scaling

In general, it is observed that intraslab rupture length, width, and area-scaling properties all yield smaller values than interface ruptures for the corresponding magnitude (Fig. 7a–c). However, the average and maximum slip distance is larger than for interface events (Fig. 7d,e). This observation is consistent with the notion that either: (a) the stress drop for intraslab events is higher (e.g., Allmann and Shearer, 2009) or that (b) the shear modulus (rigidity) is larger within downgoing, subducting slabs (e.g., Bilek and Lay, 1999). The coefficients for the intraslab-scaling relationships are provided in Table 5.

Although magnitude-dependent intraslab earthquake rupture geometry and slip do appear to vary from those of interface earthquakes, the L–W scaling remains roughly consistent between the two earthquake mechanisms when the gradient from the low-magnitude interface model is assumed (i.e., below the saturation width; Fig. 7f).

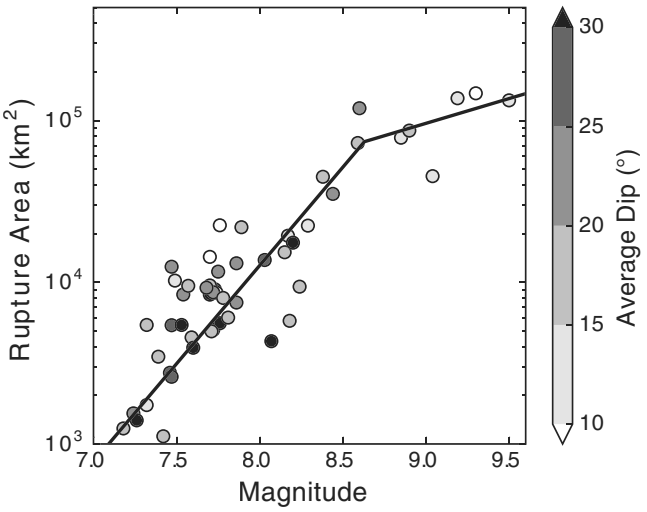

Figure 5. Interface rupture area versus magnitude. Data are color-coded by the average dip of the rupture interface.

A comparison of these intraslab-scaling relations with those of Strasser *et al.* (2010) reveals both relations demonstrate similar characteristics relative to the interface-scaling relations; that is, they both show smaller intraslab rupture dimensions for a given magnitude (Fig. 7a–c). However, our scaling relations yield systematically shorter rupture lengths for a given magnitude than the model of Strasser *et al.* (2010).

Other Offshore Earthquake Types

Although the focus of the present study has been on the more commonly observed subduction interface and intraslab earthquakes, a small data sample was also compiled to provide information on the rupture behavior of offshore strike-slip and extensional outer-rise earthquakes. In the recent seismological record, we witnessed several examples of each rupture type, including the M_w 8.6 2012 Indian Ocean earthquake (e.g., Duputel *et al.*, 2012; Yue *et al.*, 2012) and the M_w 8.1 2007 Kuril Islands earthquake (Ammon *et al.*, 2008), respectively. However, to our knowledge, no information on the appropriate source scaling for these two faulting types exists in the context of their oceanic settings.

Using the fixed gradients obtained from the interface regression analyses, visual examination of the length and width scaling for offshore strike-slip ruptures suggests that these earthquakes generate longer rupture lengths relative to interface earthquakes and significantly narrower ruptures (Figs. 7a,b). The latter observation is likely a consequence of thinner oceanic crust (e.g., Mooney *et al.*, 1998) that is available to rupture (though some recent oceanic strike-slip earthquakes seem to have ruptured into the oceanic mantle; e.g., Duputel *et al.*, 2012). Thus, in order for magnitude to increase, the earthquake ruptures appear to have much larger slip, both D_{av} and D_{max} (e.g., equation 9).

Although it may typically be expected that oceanic strike-slip earthquakes should not have vertically dipping ruptures any thicker than typical oceanic crustal settings (~10 km), some evidence suggests that these earthquakes can extend through the thin oceanic crust into the upper mantle below (Duputel *et al.*, 2012), generating wider ruptures. The model developed for oceanic strike-slip earthquakes allows rupture width up to ~40 km for larger events (up to M_w 8.6). The maximum and average slip characteristics of offshore strike-slip earthquake ruptures indicate significantly larger values than both interface and in-slab earthquakes (Fig. 7d,e). However, comparing each of the rupture-scaling metrics for offshore strike-slip earthquakes examined herein with the commonly used Wells and Coppersmith (1994) scaling relationships suggests that these ruptures behave similarly to onshore strike-slip earthquakes (Fig. 7). In the absence of abundant rupture data from offshore strike-slip earthquakes, these results suggest that rupture-scaling relationships developed for shallow crustal events (e.g., Wells and Coppersmith, 1994, and others) may be adequate to use as a proxy in oceanic environments. The coefficients for the oceanic strike-slip earthquakes are presented in Table 5.

Outer-rise earthquakes occur within oceanic crust that is about to be subducted, and their focal planes are typically oriented approximately parallel to the trench axes. In uncoupled subduction zones, extensional (normal faulting) earthquakes are associated with plate bending and/or slab pull forces. In strongly coupled subduction zones, both tensional and compressional (reverse faulting) outer-rise events are observed (Christensen and Ruff, 1988). While less common than interface earthquakes, outer-rise earthquakes have the potential to trigger tsunamis, which pose significant hazards to coastal communities (e.g., Satake and Tanioka, 1999). Consequently, it is necessary to understand the rupture properties of these events, and their uncertainties, so that they can be modeled in both a probabilistic tsunami- and seismic-hazard framework, as well as for scenario tsunami inundation modeling.

Among the FFRMs of Hayes *et al.* (2015), a small number (four) of outer-rise earthquakes are present. Constraining the gradient of the regression coefficients from the interface relations, initial scaling relationships are derived for outer-rise earthquakes. Both the width and area scaling of outer-rise ruptures tend to yield lower values than for equivalently sized interface events (Fig. 7b,c). In contrast, the slip metrics yield larger values for a given magnitude, which is required to conserve seismic moment (equation 9). The coefficients for the oceanic outer-rise earthquakes are presented in Table 5.

Evaluation of Finite-Fault Trimming Method

With the exception of the relationship for D_{max}, the scaling relationships presented herein are necessarily dependent on the FFRM trimming method chosen. The trimming process is necessary because rupture-model-inversion space must be chosen *a priori* to exceed the expected rupture area; thus there should be significant portions of the model that have low (or zero) slip. We investigate the performance of the previously described trimming method using crustal earth-

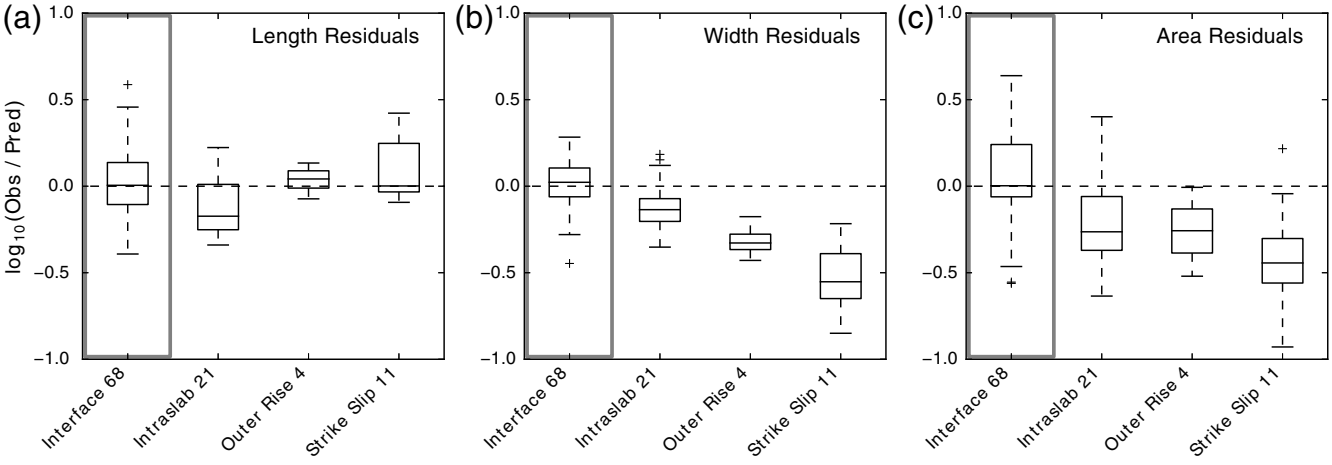

Figure 6. Box and whisker plots indicating model residuals in (a) rupture length, (b) rupture width, and (c) rupture area for different event types relative to the bilinear interface-scaling coefficients in Table 2. Rupture-scaling residuals for interface events (enclosed in solid boxes) are compared with the other rupture types. The number of events for each rupture type is indicated.

quakes, for which coseismic rupture lengths can be more reliably determined from postevent reconnaissance or through interferometric methods (e.g., interferometric synthetic aperture radar). A listing of earthquakes used for this purpose is provided in Table 6. Figure 8 shows the comparison of observed coseismic rupture lengths against those determined from the FFRMs. Figure 8 reveals an excellent correspondence between the observed and modeled rupture lengths with a standard deviation of the residuals of 0.04 log units. Relative to the standard deviation of the scaling models themselves (e.g., Table 2), the uncertainty of determining rupture dimensions from FFRMs is a minor contribution relative to the aleatory variability between earthquakes.

Discussion

The characterization of earthquake rupture models in subduction and oceanic environments carries a higher degree of uncertainty than for shallow crustal earthquakes because direct observation of surface displacement surrounding the source and of the extent of the coseismic rupture is generally not possible. Consequently, resolving the effective area that generates large displacements and strong ground motions is a challenging task. Prior to the advent of FFRM techniques, rupture geometries for large offshore earthquakes were largely inferred from the distribution of aftershock epicenters in the days following the mainshock (e.g., Wells and Coppersmith, 1994). Although this method still provides a rapid and useful validation of FFRMs, the distribution of aftershocks may not accurately represent the true rupture area or the region of strong-motion generation from the mainshock.

Table 4
Rupture-Scaling Residual Statistics by Event Type Relative to the Preferred Interface-Type Coefficients

	Event Type	$\tilde{\Delta}$	σ	p-value
Rupture-length residuals	Intraslab	−0.17	0.16	0.001
	Outer rise	0.04	0.08	0.797
	Strike slip	0.00	0.17	0.218
Rupture-width residuals	Intraslab	−0.14	0.14	0.000
	Outer rise	−0.33	0.09	0.005
	Strike slip	−0.55	0.19	0.000
Rupture-area residuals	Intraslab	−0.26	0.26	0.000
	Outer rise	−0.26	0.19	0.057
	Strike slip	−0.44	0.30	0.000

The median ($\tilde{x}$), standard deviation (σ), and p-value of the $\log_{10}$ rupture-scaling residuals by event type relative to interface event type scaling coefficients in Table 2.

Exploration of the scatter between alternative subduction interface-length-scaling linear (L) relationships from various authors suggests that most of the models broadly agree (Fig. 3a). However, there is significant scatter among published width- and area-scaling models (Fig. 3b,c). A key factor driving the difference in rupture scaling is the assumption of either linear (e.g., Blaser *et al.*, 2010; Leonard, 2010; Strasser *et al.*, 2010) or width-limited bilinear scaling (e.g., Skarlatoudis *et al.*, 2016; this study). Those models that assume a linear W–M_w generally predict narrower rupture widths for interface events at lower magnitudes and larger rupture widths for great-sized earthquakes (approximately $M_w \geq 8.7$). Despite the independent nature of the datasets used to derive their relationships, there is good agreement between the rupture-width saturation of subduction interface earthquakes between the Skarlatoudis *et al.* (2016) bilinear rupture-width scaling model and the model proposed herein.

In contrast to other published relationships, the model herein proposes bilinear interface magnitude-area rupture scaling. The bilinear parameterization yields larger areas of significant ground-motion generation for smaller magnitude events than predicted by alternative relationships (approximately M_w 8.0–8.8) but generally suggests smaller rupture areas for great-sized earthquakes (Fig. 3c). Notably, the bilinear area-scaling model suggests that the area of strong ground motion generation is less well correlated to magnitude above M_h. This suggests that fault segments with

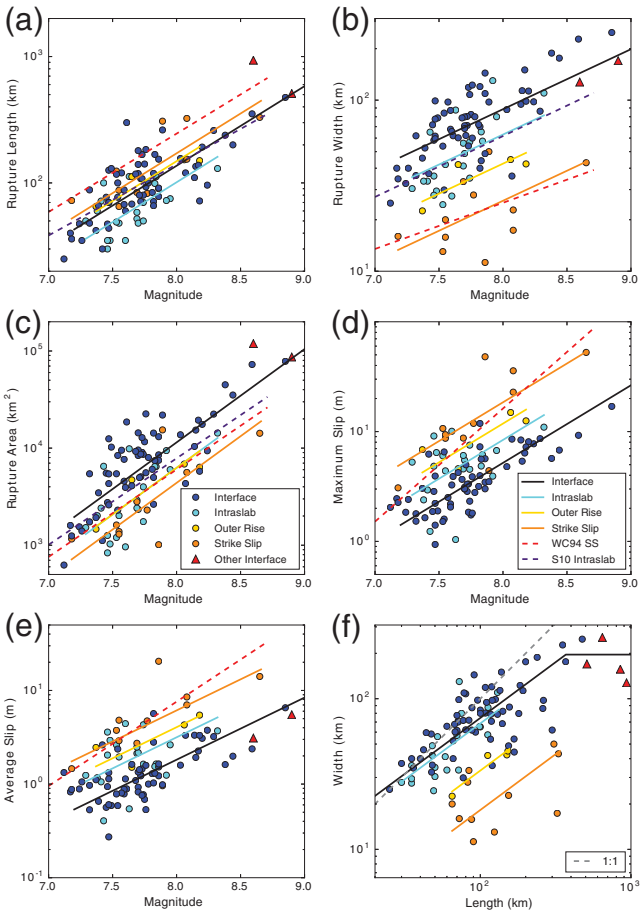

Figure 7. Orthogonal regressions for other offshore rupture types. Relationships are shown between earthquake magnitude M_w and (a) rupture length L, (b) rupture width W, (c) rupture area S, (d) maximum slip D_{max}, and (e) average slip D_{av}. (f) Length–width scaling is also shown together with 1:1 L–W scaling (gray dashed line). Where applicable, the Strasser *et al.* (2010; S10 intraslab) scaling relations are shown for in-slab earthquake ruptures, as well as the Wells and Coppersmith (1994; WC94 SS) relationship for crustal strike-slip ruptures.

relatively smaller asperity areas have the potential to generate great-magnitude earthquakes ($M_w > 9.0$) than might be predicted by existing area-magnitude scaling relationships. The occurrence of these great-magnitude events assumes that the average slip across the rupture surface continues to grow with magnitude. This effect was recently demonstrated through the 2011 M_w 9.0 Tohoku earthquake, which had significantly smaller rupture dimensions than had previously been observed for an earthquake of its magnitude.

There is clearly a trade-off between the complexity of the model and its ability to predict real-world observations. Consequently, one must weigh the improved predictive power of our four-coefficient bilinear model against the simpler two-coefficient model used for both rupture width and rupture area. Akaike information criterion (AIC; Akaike, 1973) is a measure of the relative quality of one or more statistical models to a given dataset. The method is often used to determine the relative likelihood (e.g., Wagenmakers and Farrell, 2004) of candidate models by comparing the overall fit, as well as the complexity, of any given model. Here, we examine the relative quality of the linear W_1 and bilinear W_2 width-scaling models. Using the full dataset, the W_1 width-scaling model was determined to have a marginally better AIC value than the W_2 model (−68.4 relative to −67.7), with the bilinear model being 71% as likely as the linear fit to model the rupture-width data. However, if we only consider earthquakes of magnitude $M_w \geq 8.0$, which are less abundant in the dataset but more important (see Fig. 2b), the four-coefficient bilinear parameterization is 92% as likely as the two-coefficient linear parameterization to model the rupture-width data.

Although these tests suggest there may be limited benefit in using a more complex model, statistical measures of likelihood can only be so effective in assessing the quality of a model and often cannot capture real-world complexities in earthquake source physics. These likelihood metrics must be placed in the context of the physical world, in which down-dip rupture widths, continuing to grow with increasing magnitude, become less likely owing to the thermal properties of subduction interfaces (e.g., Hyndman *et al.*, 1997). Consequently, given the similar AIC assessments, we continue to recommend the bilinear rupture-width model as the preferred scaling relationship with earthquake magnitude.

There are few magnitude–slip scaling relationships for interface earthquakes. The empirical model proposed herein suggests larger average (D_{av}) and maximum (D_{max}) slips for large-magnitude earthquakes than the self-similar models of Murotani *et al.* (2013) and Skarlatoudis *et al.* (2016) (Fig. 3d,e). This appears to be consistent with FFRMs from recent megathrust earthquakes (e.g., the great-sized 2004 M_w 9.2 Sumatra–Andaman Islands and 2011 M_w 9.0 Tohoku earthquakes).

The most-commonly applied intraslab-specific rupture-scaling model is that of Strasser *et al.* (2010). Their model and those proposed herein generally show similar characteristics relative to interface scaling relationships (Fig. 7a–c). That is, they both show smaller rupture dimensions for a given magnitude for intraslab events. The relationships proposed herein also provide rupture-slip scaling, which shows greater maximum and average slip for intraslab events (Fig. 7d–f), which is required to conserve seismic moment given the smaller rupture geometries (equation 9). This is consistent with the notion that intraslab earthquakes generally have higher stress drops than interface events. Because intraslab earthquakes are generally not expected to grow much beyond M_w 8.0 (because they are typically limited to the thickness of the subducting slab, with the exception of rare, multifault ruptures like the 2013 M_w 8.3 Okhotsk earthquake), only linear scaling models are proposed.

Based on the sparse dataset of offshore strike-slip-faulting earthquake rupture models gathered herein, we observe similar rupture scaling to that observed from onshore strike-slip earthquakes from other studies (Fig. 7). Because of the small sample dataset of 11 earthquakes, and their apparent similar behavior to the rupture scaling observed for

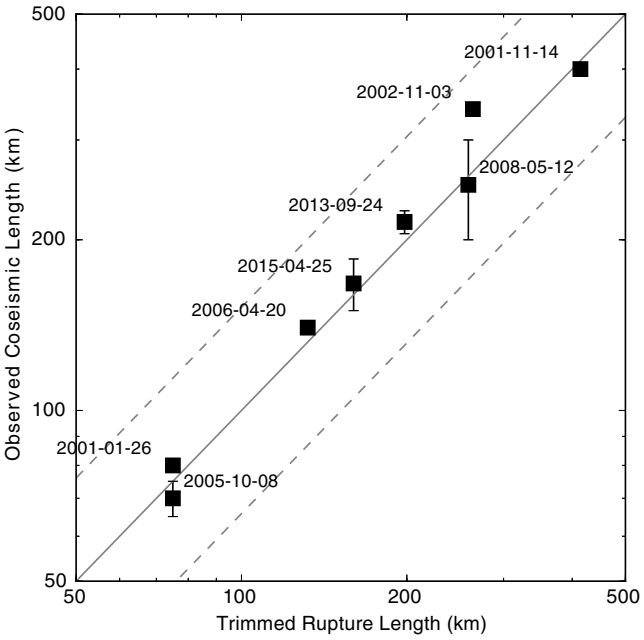

Figure 8. Comparison of observed coseismic rupture lengths against those determined from the FFRMs. For reference, the dashed lines indicate the standard deviation from the M_w–L scaling model for subduction earthquakes (Table 2). Each data point is annotated with the earthquake's date.

onshore strike-slip events, it may be prudent to assume rupture-scaling properties of those existing relationships that are defined based on much larger datasets of onshore coseismic ruptures (e.g., Wells and Coppersmith, 1994; Hanks and Bakun, 2002; and others). Although from only a small sample size, it is interesting to note the large differences in rupture area and slip for our offshore strike-slip earthquakes relative to interface-rupturing events, suggesting that the offshore strike-slip events possess significantly higher stress drops. Similarly, while also derived from a small dataset, the rupture scaling indicated for outer-rise earthquakes suggests narrower rupture widths than do interface earthquakes of the same size, but larger average slips (Fig. 7).

As previously discussed, the scaling relationships presented herein are necessarily dependent on the FFRM and the trimming method chosen (with the exception of the relationship for D_{max}). The aforementioned method used in this study was designed to be both repeatable and to preserve the area of fault rupture capable of strong ground motion and tsunami-wave generation. Mai and Beroza (2000) derive effective rupture dimensions from the autocorrelation of the slip function as an alternative trimming procedure. The change in length following the trimming process in the present study is generally consistent with Mai and Beroza (2000). Other studies developed alternative logic to capture fault parameters. The Next Generation Attenuation project used a preferential logic based on: (1) field observations of coseismic surface ruptures; (2) FFRMs; and (3) observations of aftershock distributions (Chiou *et al.*, 2008). When FFRMs are used, Chiou *et al.* (2008) recommends that regions of more than 50 cm of coseismic slip should not be trimmed. In this study, we do not follow this convention because the resolution of the FFRMs for offshore earthquakes is generally not as accurate as for the crustal earthquakes considered by Chiou *et al.* (2008). In another study exploring the recorded ground-motion field from the 2011 Tohoku earthquake (Stewart *et al.*, 2013), the distance to seismic rupture is calculated by trimming regions of the preferred FFRM for which slip is less than 3 m. Finally, it is worth noting that

Table 5
Rupture-Scaling Coefficients for Other Offshore Earthquake Rupture Styles

	Type	a	SE_a	b*	σ_x	M_w Range
Length: $\log L = a + b \times M_w$ (km)	Inslab	−3.03	0.04	0.63	0.14	7.3–8.3
	Outer rise	−2.87	0.04		0.08	7.4–8.2
	Strike slip	−2.81	0.05		0.15	7.2–8.7
Width: $\log W = a + b \times M_w$ (km)	Inslab	−1.01	0.03	0.35	0.15	7.3–8.3
	Outer rise	−1.18	0.04		0.08	7.4–8.2
	Strike slip	−1.39	0.06		0.17	7.2–8.7
Area: $\log S = a + b \times M_w$(km^2)	Inslab	−3.89	0.06	0.96	0.19	7.3–8.3
	Outer rise	−3.89	0.08		0.11	7.4–8.2
	Strike slip	−4.04	0.08		0.2	7.2–8.7
Maximum slip: $\log D_{max} = a + b \times M_w$ (m)	Inslab	−4.73	0.05	0.71	0.21	7.3–8.3
	Outer rise	−4.58	0.08		0.14	7.4–8.2
	Strike slip	−4.39	0.08		0.21	7.2–8.7
Average slip: $\log D_{av} = a + b \times M_w$ (m)	Inslab	−4.81	0.06	0.66	0.22	7.3–8.3
	Outer rise	−4.70	0.08		0.14	7.4–8.2
	Strike slip	−4.52	0.10		0.26	7.2–8.7
Width–length: $\log W = a + b \times \log L$ (km)	Inslab	0.35	0.03	0.74	0.13	7.3–8.3
	Outer rise	0.04	0.02		0.09	7.5–8.2
	Strike slip	−0.22	0.06		0.18	7.5–8.7

All logarithms are base 10. SE_a is the standard error on the variable a.
*Gradients b determined from linear regression of interface-rupture-scaling coefficients (Table 2). The constant a is determined from orthogonal regression in all cases.

Table 6
Crustal Earthquakes Used to Evaluate the Determination of Rupture Length from the FFRMs

Date (yyyy/mm/dd)	Place	M_w	Trimmed Length (km)	Minimum Coseismic Length (km)	Maximum Coseismic Length (km)	References
2001/01/26	Bhuj, India	7.61	75	80	80	Jade *et al.* (2002)
2001/11/14	Central Kunlun, China	7.84	414	400	400	Lin *et al.* (2002)
2002/11/03	Denali, Alaska	7.97	264	340	340	Eberhart-Phillips *et al.* (2003) and Haeussler *et al.* (2004)
2005/10/08	Kashmir, Pakistan	7.57	75	65	75	Jayangondaperumal and Thakur (2008) and Chini *et al.* (2011)
2006/04/20	Koryakia, Russia	7.58	132	140	140	Rogozhin *et al.* (2009)
2008/05/12	Wenchuan, China	7.88	259	200	300	Dong *et al.* (2008) and Liu-Zeng *et al.* (2009)
2013/09/24	Balochistan, Pakistan	7.72	198	205	225	Zinke *et al.* (2014) and Zhou *et al.* (2015)
2015/04/25	Gorkha, Nepal	7.86	160	150	185	Diao *et al.* (2015) and Wang and Fialko (2015)

FFRM, finite-fault rupture model.

there are also trade-offs between D_{max} and the resolution of the subfault area chosen by the FFRM modeler. Thus the maximum slip predicted by the equations herein should only be considered as representative of the physical rupture process.

Conclusions

Using a new database of consistently derived FFRMs from teleseismic inversion, alternative rupture-scaling relationships have been developed for earthquakes in subduction (interface and intraslab) and other offshore environments. The magnitude limits and conditions of use for the equations are provided in Tables 2 and 5. Interface-rupture-scaling relationships are provided for rupture area (S), rupture length (L), rupture width (W), maximum slip (D_{max}), and average slip (D_{av}) for earthquakes between M_w 7.1 and 9.5.

Based on the observations of Hyndman *et al.* (1997), the down-dip seismogenic limit for most subduction zones appears to agree with either a maximum temperature of 350°C or the thrust intersection with the fore-arc serpentinized mantle. This suggests that there should be some lower limit to down-dip rupture extent, which appears to be consistent with the empirical data from this and other studies (e.g., Tajima *et al.*, 2013). We observe that the down-dip rupture width appears to saturate for larger-magnitude earthquakes near 200 km (196 km on average). A bilinear M_w–W scaling model is developed that reflects this magnitude saturation of rupture width (Fig. 3b). Unlike other existing subduction interface-rupture-scaling relations, we also assume bilinear M_w–S scaling. This relationship yields larger rupture areas for magnitudes between approximately M_w 8.0 and 8.8, but smaller areas at large magnitudes (Fig. 3c). Furthermore, this bilinear area-scaling model suggests that fault asperity area is less well correlated with magnitude for earthquakes of $M_w > 8.6$. Consequently, the magnitude for great earthquakes appears to be more strongly controlled by the average slip across the rupture asperity. This observation may have consequences for earthquake- and tsunami-hazard assessments in which the assumed maximum earthquake magnitude may be based solely on the assumed asperity (or fault) area. Specifically, subduction interface earthquakes with larger average slip for a given asperity area would yield larger ground-motion amplitudes and would likely generate larger coseismic displacements on the ocean floor, leading to more severe tsunami waves.

The regional variability in interface-rupture-scaling characteristics, which may arise from factors such as varying slab dip, velocity, or temperature, was also investigated (Fig. 4). However, hypothesis testing currently does not support region-specific adjustment factors (Table 3). Although no significant bias in rupture scaling could be identified with the dip of the interface, a potential link between dip and the likely maximum magnitude of interface events was observed in the present FFRM dataset (which is typically limited to post-1990 events). The data suggest that great events (approximately $M_w \geq 8.0$) that nucleate on steeply dipping subduction interfaces (approximately $\geq 25°$) may occur at much lower probabilities than on shallow-dipping interfaces, particularly for regions characterized by continental subduction. Not included in our dataset is the 1985 M_w 7.96 Michoacán, Mexico, earthquake (e.g., Ekström *et al.*, 2012), which occurred in the more steeply dipping Mexico subduction zone (slab dip ~26°; Hayes *et al.*, 2012). The occurrence of the 1985 event suggests that M_w 8.0 may not be the upper magnitude limit in steeply dipping subduction environments. However, the likelihood of the occurrence of these great-sized earthquakes may be lower than in more shallowly dipping subduction zone settings.

Rupture-scaling relationships are also provided for intraslab earthquakes, as well as for offshore strike-slip and tensional outer-rise events. Because these faulting types represent a smaller population of the FFRM database, their associated models are constrained by the magnitude-scaling rates for interface events. In all cases, rupture areas tend to be smaller than for interface events of the same magnitude, with larger maximum and average slip. These observations reflect both the narrower fault widths that have the potential to rupture and likely higher stress drops.

The objective for developing rupture-scaling relationships of offshore earthquakes is to better determine the area of strong-motion generation and slip for both earthquake- and tsunami-hazard modeling. These alternative models will allow hazard modelers and practitioners to explore the epistemic uncertainty among existing rupture-scaling relations for subduction and other offshore earthquakes for a variety of applications (e.g., PSHA, PTHA, and scenario ground shaking and tsunami modeling). Furthermore, the scaling models proposed herein could be used in concert with pre-existing models of subducting slab geometries (e.g., Hayes *et al.*, 2012) to generate rapid empirical fault-rupture models for near-real-time earthquake ground-shaking and impact assessments. This approach is likely to be better—in the immediate aftermath of a large earthquake, and prior to the availability of a teleseismic inversion-based FFRM—than assuming a point-source rupture. Consequently, areas potentially affected by strong ground shaking could be rapidly assessed, which may facilitate improved impact assessments and response.

Data and Resources

Most finite-fault rupture models (FFRMs) used in this study were obtained from the U.S. Geological Survey's Advanced National Seismic System Comprehensive Catalog (ComCat; https://earthquake.usgs.gov/data/comcat/, last accessed February 2017), whereas others were calculated specifically for this study. Sources for rupture parameters of other interface earthquakes are referenced in the article. The SciPy ODRPACK functions were used for the orthogonal regressions. Further details on the method can be obtained from SciPy.org (last accessed February 2017).

Acknowledgments

Many thanks to Roy Hyndman, Kelin Wang, William Levandowski, and an anonymous reviewer for their thoughtful reviews of this article. Andreas Skarlatoudis is thanked for providing updated parameterization for the Somerville *et al.* (2015) non-self-similar L and W scaling models.

References

Akaike, H. (1973). Information theory as an extension of the maximum likelihood principle, in B. N. Petrov and F. Csaki (Editors), *Second International Symposium on Information Theory*, Akaemiai Kiado, Budapest, Hungary, 267–281.

Aki, K. (1966). Generation and propagation of G waves from the Niigata earthquake of June 16, 1964. Part 2. Estimation of earthquake moment, released energy, and stress-strain drop from the G wave spectrum, *Bull. Earthq. Res. Inst.* **44,** 73–88.

Allen, T. I., and G. P. Hayes (2015). Subduction interface fault scaling relationships to facilitate rapid ground-shaking and impact assessments, *Seismol. Res. Lett.* **86,** no. 2B, 618.

Allmann, B. P., and P. M. Shearer (2009). Global variations of stress drop for moderate to large earthquakes, *J. Geophys. Res.* **114,** no. B01310, doi: 10.1029/2008JB005821.

Ammon, C. J., H. Kanamori, and T. Lay (2008). A great earthquake doublet and seismic stress transfer cycle in the central Kuril Islands, *Nature* **451,** 561–565, doi: 10.1038/nature06521.

Bilek, S. L., and T. Lay (1999). Rigidity variations with depth along interplate megathrust faults in subduction zones, *Nature* **400,** 443–446, doi: 10.1038/22739.

Blaser, L., F. Krüger, M. Ohrnberger, and F. Scherbaum (2010). Scaling relations of earthquake source parameter estimates with special focus on subduction environment, *Bull. Seismol. Soc. Am.* **100,** 2914–2926, doi: 10.1785/0120100111.

Chini, M., F. R. Cinti, and S. Stramondo (2011). Co-seismic surface effects from very high resolution panchromatic images: The case of the 2005 Kashmir (Pakistan) earthquake, *Nat. Hazards Earth Syst. Sci.* **11,** 931–943, doi: 10.5194/nhess-11-931-2011.

Chiou, B., R. Darragh, N. Gregor, and W. Silva (2008). NGA project strong-motion database, *Earthq. Spectra* **24,** 23–44, doi: 10.1193/1.2894831.

Christensen, D. H., and L. J. Ruff (1988). The seismic coupling of outer rise earthquakes, *J. Geophys. Res.* **93,** 13,421–13,444, doi: 10.1029/JB093iB11p13421.

Diao, F., T. R. Walter, M. Motagh, P. Prats-Iraola, R. Wang, and S. V. Samsonov (2015). The 2015 Gorkha earthquake investigated from radar satellites: Slip and stress modeling along the MHT, *Front. Earth Sci.* **3,** doi: 10.3389/feart.2015.00065.

Dong, S., Y. Zhang, Z. Wu, N. Yang, Y. Ma, W. Shi, Z. Chen, C. Long, and M. An (2008). Surface rupture and co-seismic displacement produced by the M_S 8.0 Wenchuan earthquake of May 12th, 2008, Sichuan, China: Eastwards growth of the Qinghai-Tibet plateau, *Acta Geol. Sin.* **82,** 938–948, doi: 10.1111/j.1755-6724.2008.tb00649.x.

Duputel, Z., H. Kanamori, V. C. Tsai, L. Rivera, L. Meng, J.-P. Ampuero, and J. M. Stock (2012). The 2012 Sumatra great earthquake sequence, *Earth Planet. Sci. Lett.* **351/352,** 247–257, doi: 10.1016/j.epsl.2012.07.017.

Eberhart-Phillips, D., P. J. Haeussler, J. T. Freymueller, A. D. Frankel, C. M. Rubin, P. Craw, N. A. Ratchkovski, G. Anderson, G. A. Carver, A. J. Crone, *et al.* (2003). The 2002 Denali fault earthquake, Alaska: A large magnitude, slip-partitioned event, *Science* **300,** 1113–1118, doi: 10.1126/science.1082703.

Ekström, G., M. Nettles, and A. M. Dziewoński (2012). The global CMT project 2004–2010: Centroid-moment tensors for 13,017 earthquakes, *Phys. Earth Planet. In.* **200/201,** 1–9, doi: 10.1016/j.pepi.2012.04.002.

Haeussler, P. J., D. P. Schwartz, T. E. Dawson, H. D. Stenner, J. J. Lienkaemper, B. Sherrod, F. R. Cinti, P. Montone, P. A. Craw, A. J. Crone, *et al.* (2004). Surface rupture and slip distribution of the Denali and Totschunda faults in the 3 November 2002 **M** 7.9 earthquake, Alaska, *Bull. Seismol. Soc. Am.* **94,** S23–S52, doi: 10.1785/0120040626.

Hanks, T. C., and W. H. Bakun (2002). A bilinear source-scaling model for **M**-log A observations of continental earthquakes, *Bull. Seismol. Soc. Am.* **92,** 1841–1846, doi: 10.1785/0120010148.

Hayes, G. P., H. M. Benz, and W. D. Barnhart (2015). Near realtime, multi-approach earthquake source inversion, and an extensive, consistent finite fault database, *Seismol. Res. Lett.* **86,** no. 2B, 711 pp.

Hayes, G. P., D. J. Wald, and R. L. Johnson (2012). Slab1.0: A three-dimensional model of global subduction zone geometries, *J. Geophys. Res.* **117,** no. B1, doi: 10.1029/2011JB008524.

Heuret, A., S. Lallemand, F. Funiciello, C. Piromallo, and C. Faccenna (2011). Physical characteristics of subduction interface type seismogenic zones revisited, *Geochem. Geophys. Geosys.* **12,** no. Q01004, doi: 10.1029/2010GC003230.

Horspool, N., I. Pranantyo, J. Griffin, H. Latief, D. H. Natawidjaya, W. Kongko, A. Cipta, B. Bustaman, S. D. Anugrah, and H. K. Thio (2014). A probabilistic tsunami hazard assessment for Indonesia, *Nat. Hazards Earth Syst. Sci.* **2,** 3105–3122, Discussion Paper, doi: 10.5194/nhessd-2-3423-2014.

Hyndman, R. D., M. Yamano, and D. A. Oleskevich (1997). The seismogenic zone of subduction thrust faults, *Isl. Arc* **6,** 244–260, doi: 10.1111/j.1440-1738.1997.tb00175.x.

Jade, S., M. Mukul, I. A. Parvez, M. B. Ananda, P. D. Kumar, and V. K. Gaur (2002). Estimates of coseismic displacement and post-seismic deformation using Global Positioning System geodesy for the Bhuj earthquake of 26 January 2001, *Curr. Sci.* **82,** 748–752.

Jayangondaperumal, R., and V. C. Thakur (2008). Co-seismic secondary surface fractures on southeastward extension of the rupture zone of the

2005 Kashmir earthquake, *Tectonophysics* **446,** 61–76, doi: 10.1016/j.tecto.2007.10.006.

Johnson, J. M., and K. Satake (1999). Asperity distribution of the 1952 great Kamchatka earthquake and its relation to future earthquake potential in Kamchatka, *Pure Appl. Geophys.* **154,** 541–553, doi: 10.1007/978-3-0348-8679-6_8.

Johnson, J. M., K. Satake, S. R. Holdahl, and J. Sauber (1996). The 1964 Prince William Sound earthquake: Joint inversion of tsunami and geodetic data, *J. Geophys. Res.* **101,** 523–532, doi: 10.1029/95JB02806.

Johnson, J. M., Y. Tanioka, L. J. Ruff, K. Satake, H. Kanamori, and L. R. Skyes (1994). The 1957 great Aleutian earthquake, *Pure Appl. Geophys.* **142,** 3–28, doi: 10.1007/BF00875966.

Leonard, M. (2010). Earthquake fault scaling: Self-consistent relating of rupture length, width, average displacement, and moment release, *Bull. Seismol. Soc. Am.* **100,** 1971–1988, doi: 10.1785/0120090189.

Lin, A., F. Fu, J. Guo, Q. Zeng, G. Dang, W. He, and Y. Zhao (2002). Co-seismic strike-slip and rupture length produced by the 2001 M_s 8.1 Central Kunlun earthquake, *Science* **296,** 2015–2017, doi: 10.1126/science.1070879.

Liu-Zeng, J., Z. Zhang, L. Wen, P. Tapponnier, J. Sun, X. Xing, G. Hu, Q. Xu, L. Zeng, L. Ding, *et al.* (2009). Co-seismic ruptures of the 12 May 2008, M_s 8.0 Wenchuan earthquake, Sichuan: East–west crustal shortening on oblique, parallel thrusts along the eastern edge of Tibet, *Earth Planet. Sci. Lett.* **286,** 355–370, doi: 10.1016/j.epsl.2009.07.017.

Mai, M., and G. C. Beroza (2000). Source scaling properties from finite-fault-rupture models, *Bull. Seismol. Soc. Am.* **90,** 604–615, doi: 10.1785/0119990126.

Mai, M., and K. K. S. Thingbaijam (2014). SRCMOD: An online database of finite-fault rupture models, *Seismol. Res. Lett.* **85,** 1348–1357, doi: 10.1785/0220140077.

Mooney, W. D., G. Laske, and T. G. Masters (1998). CRUST 5.1: A global crustal model at 5° × 5°, *J. Geophys. Res.* **103,** 727–747, doi: 10.1029/97JB02122.

Moreno, M. S., J. Bolte, J. Klotz, and D. Melnick (2009). Impact of megathrust geometry on inversion of coseismic slip from geodetic data: Application to the 1960 Chile earthquake, *Geophys. Res. Lett.* **36,** L16310, doi: 10.1029/2009GL039276.

Murotani, S., H. Miyake, and K. Koketsu (2008). Scaling of characterized slip models for plate-boundary earthquakes, *Earth Planets Space* **60,** 987–991, doi: 10.1186/BF03352855.

Murotani, S., K. Satake, and Y. Fujii (2013). Scaling relations of seismic moment, rupture area, average slip, and asperity size for $M \sim 9$ subduction-zone earthquakes, *Geophys. Res. Lett.* **40,** 5070–5074, doi: 10.1002/grl.50976.

Pagani, M., D. Monelli, G. Weatherill, L. Danciu, H. Crowley, V. Silva, P. Henshaw, R. Butler, M. Nastasi, L. Panzeri, *et al.* (2014). OpenQuake Engine: An open hazard (and risk) software for the Global Earthquake Model, *Seismol. Res. Lett.* **85,** 692–702, doi: 10.1785/0220130087.

Rhie, J., D. Dreger, R. Bürgmann, and B. Romanowicz (2007). Slip of the 2004 Sumatra–Andaman earthquake from joint inversion of long-period global seismic waveforms and GPS static offsets, *Bull. Seismol. Soc. Am.* **97,** S115–S127, doi: 10.1785/0120050620.

Rogozhin, E. A., A. N. Ovsyuchenko, A. V. Marakhanov, and S. S. Novikov (2009). Tectonic position and geological manifestations of the 2006 Olyutor earthquake in Koryakia, *Geotectonics* **43,** 443, doi: 10.1134/S0016852109060016.

Satake, K., and Y. Tanioka (1999). Sources of tsunami and tsunamigenic earthquakes in subduction zones, *Pure Appl. Geophys.* **154,** 467–483, doi: 10.1007/978-3-0348-8679-6_5.

Schellart, W. P., and N. Rawlinson (2013). Global correlations between maximum magnitudes of subduction zone interface thrust earthquakes and physical parameters of subduction zones, *Phys. Earth Planet. In.* **225,** 41–67, doi: 10.1016/j.pepi.2013.10.001.

Skarlatoudis, A. A., P. G. Somerville, and H. K. Thio (2016). Source-scaling relations of interface subduction earthquakes for strong ground motion and tsunami simulation, *Bull. Seismol. Soc. Am.* **106,** no. 4, 1652, doi: 10.1785/0120150320.

Somerville, P., A. Skarlatoudis, and H. K. Thio (2015). Source scaling relations of subduction earthquakes for strong ground motion and tsunami prediction, *URS Group, Inc. Award Number: G13AP00028*, 25 pp.

Sørensen, M., M. Spada, A. Babeyko, S. Wiemer, and G. Grünthal (2012). Probabilistic tsunami hazard in the Mediterranean Sea, *J. Geophys. Res.* **117,** no. B01305, doi: 10.1029/2010JB008169.

Stewart, J. P., S. Midorikawa, R. W. Graves, K. Khodaverdi, T. Kishida, H. Miura, Y. Bozorgnia, and K. W. Campbell (2013). Implications of the M_w 9.0 Tohoku-Oki earthquake for ground motion scaling with source, path, and site parameters, *Earthq. Spectra* **29,** S1–S21, doi: 10.1193/1.4000115.

Strasser, F. O., M. C. Arango, and J. J. Bommer (2010). Scaling of the source dimensions of interface and intraslab subduction-zone earthquakes with moment magnitude, *Seismol. Res. Lett.* **81,** 941–950, doi: 10.1785/gssrl.81.6.941.

Tajima, R., Y. Matsumoto, and K. Irikura (2013). Comparative study on scaling relations of source parameters for great earthquakes in inland crusts and on subducting plate-boundaries, *Zisin* **66,** 31–45, doi: 10.4294/zisin.66.31 (in Japanese with English abstract).

Thio, H.-K., and W. Li (2015). Probabilistic tsunami hazard analysis of the Cascadia subduction zone and the role of epistemic uncertainties and aleatory variability, *11th Canadian Conf. on Earthquake Engineering*, Victoria, Canada, Paper 98815.

Wagenmakers, E.-J., and S. Farrell (2004). AIC model selection using Akaike weights, *Psychon. Bull. Rev.* **11,** 192–196, doi: 10.3758/BF03206482.

Wang, K., and Y. Fialko (2015). Slip model of the 2015 M_w 7.8 Gorkha (Nepal) earthquake from inversions of ALOS-2 and GPS data, *Geophys. Res. Lett.* **42,** 7452–7458, doi: 10.1002/2015GL065201.

Wells, D. L., and K. J. Coppersmith (1994). New empirical relationships among magnitude, rupture length, rupture width, rupture area, and surface displacement, *Bull. Seismol. Soc. Am.* **84,** 974–1002.

Ye, L., T. Lay, H. Kanamori, and L. Rivera (2016). Rupture characteristics of major and great ($M_w \geq 7.0$) megathrust earthquakes from 1990 to 2015: 1. Source parameter scaling relationships, *J. Geophys. Res.* **121,** 826–844, doi: 10.1002/2015JB012426.

Yue, H., T. Lay, and K. D. Koper (2012). En échelon and orthogonal fault ruptures of the 11 April 2012 great intraplate earthquakes, *Nature* **490,** 245–249, doi: 10.1038/nature11492.

Zhou, Y., J. R. Elliott, B. Parsons, and R. T. Walker (2015). The 2013 Balochistan earthquake: An extraordinary or completely ordinary event? *Geophys. Res. Lett.* **42,** doi: 10.1002/2015GL065096.

Zinke, R., J. Hollingsworth, and J. F. Dolan (2014). Surface slip and off-fault deformation patterns in the 2013 M_w 7.7 Balochistan, Pakistan earthquake: Implications for controls on the distribution of near-surface coseismic slip, *Geochem. Geophys. Geosys.* **15,** 5034–5050, doi: 10.1002/2014GC005538.

Pacific Geoscience Centre
Natural Resources Canada
9860 West Saanich Road
Sidney, British Columbia
Canada V8L 4B2
trevor.allen@ga.gov.au
(T.I.A.)

National Earthquake Information Center
U.S. Geological Survey
PO Box 25046, MS-966
Denver, Colorado 80225
ghayes@usgs.gov
(G.P.H.)

Manuscript received 8 August 2016;
Published Online 21 March 2017